



Alkyne bridge engineering of donor- π -acceptor polymers for efficient CO₂ reduction to CH₄ and C₂H₄ under visible light illumination

Guoen Tang ^a, Xiaoyan Huang ^a, Ting Song ^{a,*}, Shiheng Yin ^c, Bei Long ^a, Guo-Jun Deng ^{a,b,**}

^a Key Laboratory for Green Organic Synthesis and Application of Hunan Province, Key Laboratory of Environmentally Friendly Chemistry and Application of Ministry of Education, College of Chemistry, Xiangtan University, Xiangtan 411105, PR China

^b School of Chemistry and Chemical Engineering, Henan Normal University, Xinxiang 453007, PR China

^c Analytical and Testing Center, South China University of Technology, Guangzhou 510640, PR China



ARTICLE INFO

Keywords:

Donor- π -acceptor
Cyclotriphosphonitrile-based
CO₂ reduction
Alkyne bridge
Visible light illumination

ABSTRACT

Developing a conjugated polymer (CPs) for the formation of multi electron products or even C₂ products from CO₂ while simultaneously suppressing the 2-electron product (CO) is crucial for the efficient utilization of solar power. Herein, we investigated the donor- π -acceptor (D- π -A) CPs using cyclotriphosphonitrile, benzene and alkyne groups as the donor part, acceptor section and π -bridge structure, respectively. The photoinduced carrier separation and reduction capability of CPs can be well regulated by changing the number of π -bridges between the D and A units. Among them, three π -bridges (TTB-PCT) exhibit excellent CO₂ reduction to CH₄ (17.2 mmol g⁻¹) or C₂H₄ (0.72 mmol g⁻¹) activity under visible light illumination, which was obviously higher than two π -bridges (DTB-PCT) and four π -bridges (TTTB-PCT). TTB-PCT also exhibits excellent cycling stability (50 h). This research exhibits an innovative approach to exploit efficient metal-free CPs for photo-conversion CO₂ into multi-electron products driven by visible light.

1. Introduction

A crucial issue in relation to climatic and environmental changes is the ongoing acceleration of CO₂ emissions caused by the intensive use of fossil fuels [1]. CO₂ is one of the most stable and chemically inactive molecules, and despite the huge efforts and development made in the past decade, photocatalytic CO₂ reduction still faces enormous problems linked to the reaction activity [2,3]. The C-C coupling products, such as ethylene (C₂H₄), are the more attractive ones among all the potential CO₂ reduction products because of their higher energy densities and financial benefits [4,5]. The effective manufacture of mult carbon (C₂+) compounds has only occasionally been accomplished due to the low productivity of multielectron reduction and the slow kinetics for C-C building [6,7]. Nevertheless, the products of photocatalytic CO₂ reduction reported currently are primarily limited to C1 products (e.g., CO, CH₃OH, and HCOOH) [8]. In the mechanism of C2+ generation, *CO (*denotes adsorption site) intermediate adsorbed on the active sites has been widely recognized as one of the key reaction intermediates in the generation of C2+ products by *CO-*CO or *OC-CHOH coupling

[9]. However, when *CO undergoes C-C coupling, this process does not inevitably produce two-electron CO products, which is not favorable for efficient electron utilization [10]. If the desorption process of *CO can be significantly suppressed and protonated continuously until the *CH₂ intermediate is produced, its coupling or non-coupling will all yield multi-electron products (CH₄, C₂H₄, e.g.) without the production of the two-electron product (CO).

The introduction of metal active centers is crucial for achieving C-C coupling in both electrocatalysis and photocatalysis, especially Cu and Fe elements have been widely studied as active centers [11]. However, due to the problems of poor stability, easy poisoning, cross effect and more expensive of metals, there is an urgent need to construct the conjugated polymers (CPs) catalyst with a non-metal as the active center. CPs are desirable photocatalysts because of their extensive π -conjugation, outstanding physical and chemical stability, controllable chemical composition, and photo-electronic characteristic [12,13]. Cyclotriphosphonitrile with an electron-rich structure (P = N) as Lewis base center was recently found to be a promising unit for replacing metal active centers [14], which could serve as a fundamental point for

* Corresponding author.

** Corresponding author at: Key Laboratory for Green Organic Synthesis and Application of Hunan Province, Key Laboratory of Environmentally Friendly Chemistry and Application of Ministry of Education, College of Chemistry, Xiangtan University, Xiangtan 411105, PR China.

E-mail addresses: songtg@xtu.edu.cn (T. Song), gjdeng@xtu.edu.cn (G.-J. Deng).

capturing CO₂ molecules, optimizing the efficiency of charge separation and promoting the dimerization of intermediates. Additionally, a number of approaches have been proposed to improve the photocatalytic ability of CPs, including extending the wavelength of absorption range, constructing organic-inorganic or organic-organic heterojunctions [15], developing donor-acceptor (D-A) or donor- π -acceptor (D- π -A) structures [16,17], and boosting the hydrophilic properties.

Constructing D-A or D- π -A type CPs has garnered a lot of interest among these methods because the inherent electronic push-pull force between D groups and A groups is beneficial in aiding the photoinduced separation of charges and hence boosting the photocatalytic efficiency of CPs [18,19]. When compared to the D-A structure, D- π -A structures using greater π -electron delocalization can increase the exciton dissolution and reduced exciton binding energy, thereby improving photocatalytic activity [20,21]. By employing pyrene, benzothiadiazole, and benzene as the donor group, acceptor group, and -linker units, respectively, Xu et al [16] created D- π -A CPs that have effective charge carrier transport and separation ability. However, ternary statistical conjugation is used to create the majority of D- π -A CPs with outstanding photocatalytic activity, which usually would have defined the distribution of π bridge, and the distribution of π bridge is critical for the migration of photoinduced carriers as the only electron bridge between the D-A structures [22,23]. However, most D- π -A CPs are concerned with the modulation of the D- or A-units, and detailed modulation of the π -bridges has not been reported.

Herein, we explored a simple solvothermal synthesis of D- π -A CPs in which cyclotriphosphonitrile acts as donor units (D) with benzene ring as acceptor units (A) isolated by alkyne bridges (π - π conjugate). The electron-rich heteroatom (P = N) in cyclotriphosphonitrile can also act as a Lewis base sites to adsorb CO₂ and key intermediates (*CH₂), thus providing a site for C-C coupling. The photoinduced carrier separation and reduction capability of CPs can be well regulated by changing the number of π -bridges between the D and A units. Among them, three π -bridges (TTB-PCT) exhibit excellent CO₂ reduction to CH₄ activity (17.20 mmol g⁻¹) under visible light illumination, which was 7.6 and 3.6 times higher than those of two π -bridges (DTB-PCT) and four π -bridges (TTTB-PCT). By using the TTB-PCT catalyst, C-C coupling product C₂H₄ was also obtained with high generation rate of 0.72 mmol g⁻¹ with excellent cycle stability (50 h). This study is expected to offer guidance to combine the elaborate adjust of π -electron bridges in D- π -A systems.

2. Experimental section

2.1. Materials and method

1,4-dibromobenzene, 1,3,5-tribromobenzene, 1,2,4,5-tetrabromobenzene and hexachlorocyclotriphosphonitrile were obtained from Sigma-Aldrich Chemical Co. Ltd and used as such. All solvents were purchased from Hunan Hui-Hong reagent Co. LTO. All the solvents used for the synthesis were used directly without further processing according to the reported procedure. HPLC grade anhydrous acetonitrile was purchased from Sigma-Aldrich Chemical Co. Ltd and used as such for photochemical CO₂ reduction. CDCl₃ and DMSO-d₆ were purchased from Sigma-Aldrich Chemical Co. Ltd and used for ¹H and ¹³C NMR as such.

2.2. Synthesis of D- π -A CPs

All CPs were synthesized by Nucleophilic substitution between hexachlorocyclotriphosphonitrile (PCT) and other monomers (1,4-dibromobenzene (DTB), 1,3,5-Tribromobenzene (TTB) or 1,2,4,5-Tetra-bromobenzene (TTTB)). Compound PCT (0.348 g, 0.1 mmol) and TTB (0.9 g, 0.6 mmol) were taken together in a mixed solvent of dimethylsulfoxide (4 mL) and acetonitrile (16 mL). The mixture in hydrothermal reactor was heated at 180 °C for 24 h and cool naturally. The

TTB-PCT product was washed by deionized water and ethanol in turn and dry in vacuum oven. A similar synthetic and purification procedure was employed for the DTB-PCT and TTTB-PCT as well, wherein TTB was taken instead of DTB or TTTB, respectively.

2.3. Physical measurements

XRD spectra was tested on Bruker D8 X-ray with Cu K α radiation (k = 1.5418 Å) at 40 kV, 100 mA. Diffraction intensity data were collected at the 2 θ step increment of 0.01°. Transmission electron microscopy (TEM) were conducted on a JEOL JEM-2100 electron microscope. XPS spectra were recorded using Escalab 250Xi instrument with an Al K α microfocused X-ray source. ¹³C solid-state NMR data was gained on a JEOL ECZ600R/S3 spectrometer. Utilizing a Shimadzu UV-2700 spectrophotometer, UV-visible adsorption spectra were gathered. The photoluminescence (PL) emission and time-resolved transient PL decay curves were measured using an Edinburgh, UK-made FLS980. A Micromeritics ASAP 2020 nitrogen adsorption device was used to test the samples' N₂ and CO₂ adsorption and desorption properties. By using KBr discs, fourier transform infrared (FTIR) spectra are acquired from a Nicolet 6700 spectrometer. Using Mettler-Toledo Instrumentation as thermal analyzer, the thermo-gravimetric analysis (TGA) was carried on a Shimadzu DTG-60 H thermogravimetric analyzer in air and the temperature change rate at 10 °C min⁻¹.

2.4. Photocatalytic CO₂ reduction

In a typical experiment, a photocatalytic reactor contains solution (1 mL TEOA, 2 mL H₂O and 4 mL CH₃CN or 7 mL H₂O) and the prepared CPs. After adding the reaction material to the reactor and sealing it, high purity carbon dioxide was used to conduct a continuous gas exchange operation to reach normal pressure. Following the gas exchange, the reactor was once more sealed, and an artificial visible light source stimulated by a xenon lamp (Beijing PerfectLight Co., Ltd., China) with a cut-off filter ($\lambda > 420$ nm) was used for the light experiment. Gas chromatographs (GC7900, Tian Mei, Shanghai, and GC9790II, FuLi, China) were used for gas product detection. A heat conductivity sensor and a hydrogen-based fire ionization device coupled in series are installed on the chromatograph.

2.5. Electrochemical characterization

In the DH7000 electrochemical workstation, all electrochemical analyses (photocurrent, Mott Schottky, and EIS) have been carried out in 0.2 M of sodium sulfate solution using the conventional three electrode structure. ITO glass plates with catalyst slurry coating are used as working electrodes, platinum foil can be used as counter electrode and saturated Ag/AgCl can be used as reference electrode. The used voltage was maintained at 0.2 V during the photocurrent test while being illuminated by visible light.

3. Results and discussion

3.1. Composition and structure

Three D- π -A CPs with tunable acetylene bridges, namely DTB-PCT, TTB-PCT and TTTB-PCT, were synthesized by nucleophilic substitution reactions of phosphonitrile with the respective alkynyl benzene monomers (1,4-diethynylbenzene, 1,3,5-triethynylbenzene and 1,2,4,5-tetraethynylbenzene) (Fig. 1a and Fig. S1). All three catalysts used cyclotriphosphonitrile with benzene and alkyne groups as the donor, acceptor and π -electron bridge, respectively, and their only distinction was the corresponding number of π -electron bridges on the benzene ring. The presence of alkyne bonds was confirmed by FT-IR analysis of the TTB-PCT sample (Fig. 1b), which detected the asymmetric stretching vibration of the C≡C bond at 2051 cm⁻¹ [24,25]. Furthermore, the

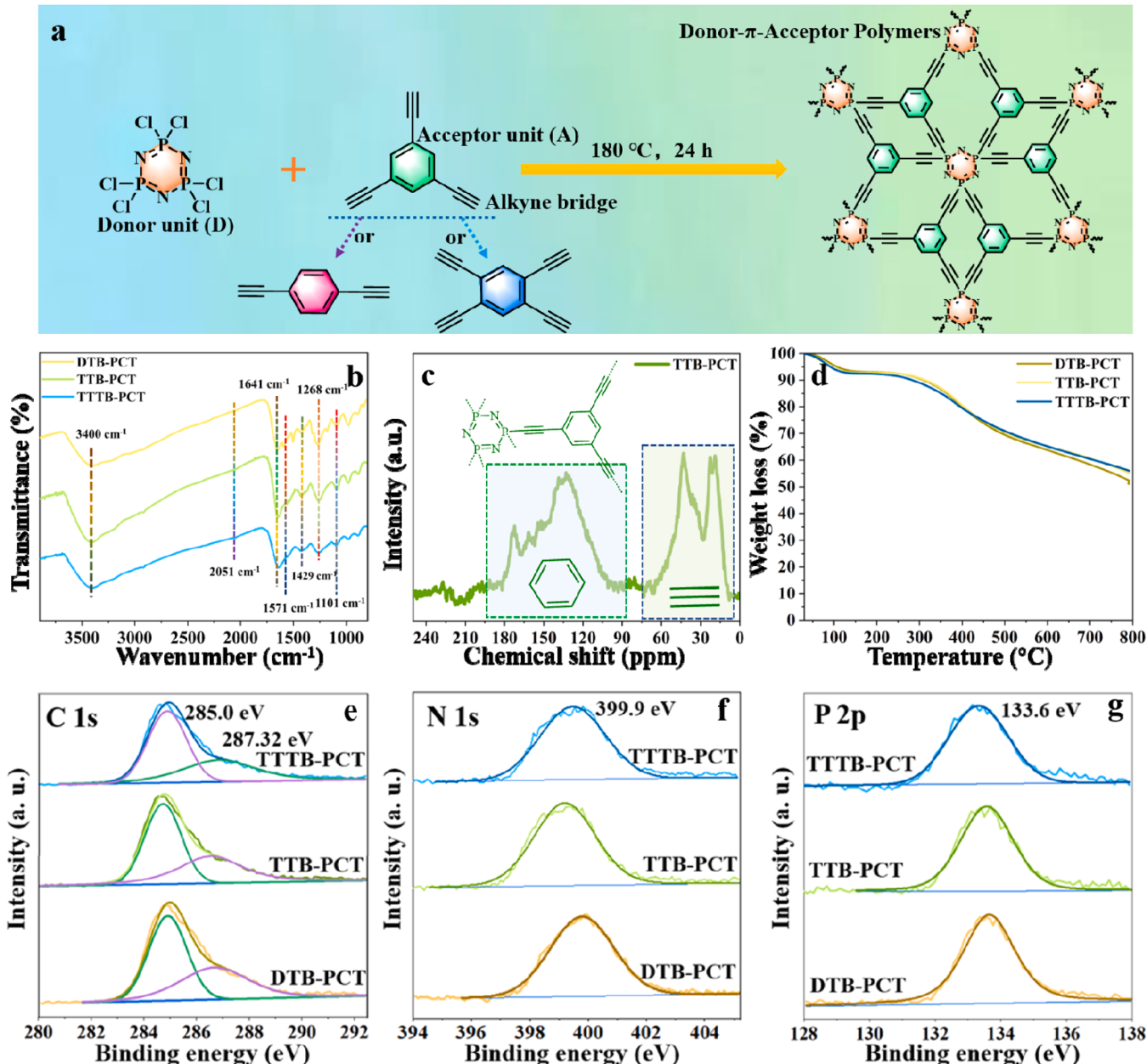


Fig. 1. (a) Synthesis of DTB-PCT, TTB-PCT and TTTB-PCT via using nucleophilic offensive reaction. (b) FT-IR spectra of DTB-PCT, TTB-PCT and TTTB-PCT. (c) Solid-state ^{13}C NMR spectrum of TTB-PCT. (d) Thermogravimetric analysis results of DTB-PCT, TTB-PCT and TTTB-PCT. XPS spectra of CPs: (e) C 1 s, (f) N 1 s, and (g) P 2p.

presence of aromatic rings was noted by the peaks at 1641 cm^{-1} and 1571 cm^{-1} , while the peaks at 1268 cm^{-1} and 1101 cm^{-1} indicated the presence of N = P bonds [26]. The formation of C-P bonds was demonstrated by the peak at 1429 cm^{-1} , and the existence of C-H bonds was verified by the peak at 3400 cm^{-1} . Similar peaks also existed in the FT-IR spectra of DTB-PCT and TTTB-PCT samples. The formation of three polymers was tentatively confirmed.

The ^{13}C solid-state NMR spectrum of TTB-PCT sample (Fig. 1c) showed peak shifts of 43.1 and 22.8 ppm for the alkyne carbon linked to the cyclotriphosphonitrile ring, while the peak shifts for the aromatic carbon were 98.9 and 183.9 ppm [27], further confirming the formation of the TTB-PCT polymer. The thermal stability of DTB-PCT, TTB-PCT and TTTB-PCT was evaluated by thermogravimetric analysis (TGA) (Fig. 1d). It was found that these three samples were stable at temperatures below 300 °C, and then a gradual weight loss (~45%) appeared when the temperature up to 800 °C. By comparing the TTB-PCT samples

and their monomers (Fig. S2), it was clear that the thermal stability of the polymerized samples was significantly improved. According to the XRD results (Fig. S3), all three catalysts exhibit an amorphous aggregated structure [28]. The existence of three elements C, N and P was certified by X-ray electron spectroscopy (XPS) data, and the chemical environment of C 1 s (Fig. 1e), N 1 s (Fig. 1f) and P 2p (Fig. 1g) was analyzed. For DTB-PCT, TTB-PCT and TTTB-PCT, the chemical environment of C, N and P are similar. The shifts of 285.0 eV and 287.32 eV were categorized as the C=C bond in benzene ring and C≡C in alkyne, respectively, while the shift of 399.9 eV implies an N-P bond and 133.6 eV represents a P = N bond [29]. All these findings indicate the successful synthesis of three catalysts.

The nanostructures and properties of TTB-PCT were studied by scanning electron microscope (SEM), transmission electron microscopy (TEM) and atomic force microscopy (AFM). SEM images (Fig. 2a, b) show that the TTB-PCT sample is spherical, and when its spherical shape

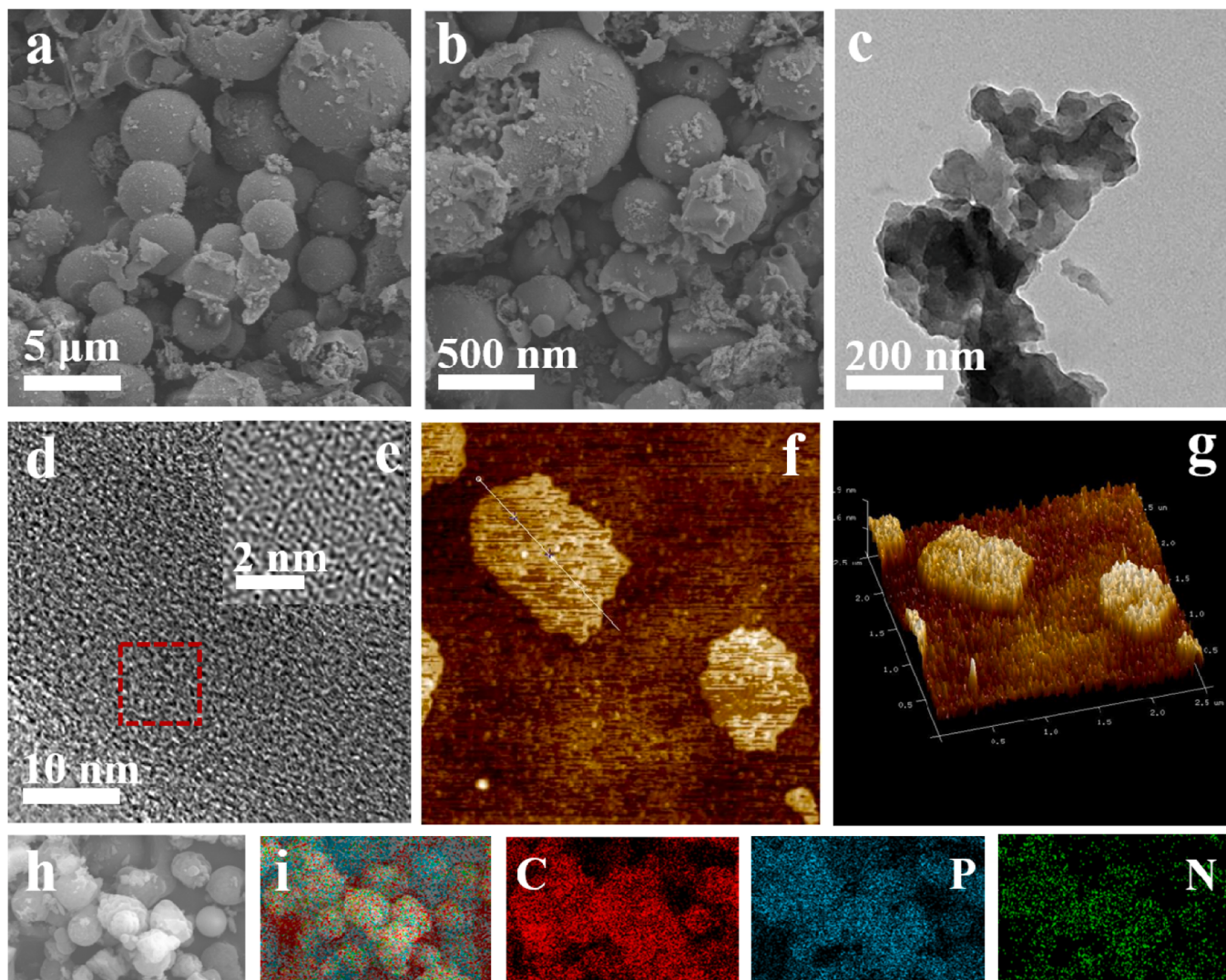


Fig. 2. SEM images of TTB-PCT (a, b). TEM images (c) and HRTEM (d, e) of TTB-PCT. (f) AFM and (g) height image of TTB-PCT. Elemental mappings of TTB-PCT (h, i) (red for C, green for N and cyan for P).

is broken, the TTB-PCT sample is lamellar, showing an ultrathin two-dimensional planarity. The TEM images (Fig. 2c) further display the ultrathin nanometric properties of the TTB-PCT samples [30]. The alternating bright and dark fields in the HRTEM images (Fig. 2d, e and S4) demonstrate the irregular micro-ring structure shown by the TTB-PCT sample, which is caused by the irregular polymerization of the electron-rich cyclotriphosphonitrile and the relatively electron-deficient 1,3,5-triethynylbenzene. The ultrathin two-dimensional (2D) planes were further demonstrated by AFM characterization (Fig. 2f and g), whose 2D heights were measured to be about a few nanometers. The elements distribution (Fig. 2h and i) of C, N and P in the TTB-PCT sample was further demonstrated by elemental mapping.

3.2. Photocatalytic CO₂ reduction performance

The photocatalytic CO₂ reduction experiments for these three samples were performed without any photosensitizer or co-catalyst under visible light illumination ($\lambda > 420$ nm). The CH₄ activity (Fig. 3a) and C₂H₄ activity (Fig. 3b) of DTB-PCT, TTB-PCT and TTTB-PCT sample increased sequentially with increasing time. The TTB-PCT sample showed excellent performance in photocatalytic CO₂ reduction, with CH₄ and C₂H₄ production values of 17.20 mmol g⁻¹ and 0.72 mmol g⁻¹ (10 h), respectively. Under the same conditions, the TTTB-PCT and DTB-

PCT samples showed CH₄ and C₂H₄ yields of 2.27 mmol g⁻¹, 4.72 mmol g⁻¹ and 0.09 mmol g⁻¹, 0.17 mmol g⁻¹, respectively (Fig. 3c). Compared to di- and tetra-alkyne bridges, the above results depend on the fact that TTB-PCT shows a suitable number of alkyne bridges, providing a higher efficiency of photogenerated carrier separation. Importantly, the yield of the optimal TTB-PCT sample is higher than most of the photocatalysts reported so far (Table S1 and S2). Control experiments demonstrated that CH₄ and C₂H₄ would not form in the absence of light, CO₂, and photocatalyst (Fig. 3d). The origin gas chromatography displayed that the gaseous product contained only CH₄, C₂H₄ and a very small amount of C₂H₆ (Fig. 3e). However, none of the three samples produced H₂ or CO. Moreover, no liquid reduction products were detected in the reaction solution as tested by ¹H NMR test (Fig. S5) [31]. The above facts indicate that all products generated by the TTB-PCT sample were multi-electron products (CH₄, C₂H₄) with a selectivity close to 100%. Photocatalytic experiments were performed with ¹³C-labeled CO₂, and the molecular weight of the generated CH₄ showed a distribution pattern of 17, 16, 15, 14 and 13 (Fig. 3f) [32], indicating that the observed product originated from CO₂. The TTB-PCT sample shows an apparent quantum efficiency (AQY) of up to 2.81% at 420 nm (Fig. 3g). In contrast, the AQY at 460 and 560 nm present 1.85% and 0.56%, respectively. Moreover, the TTB-PCT sample exhibited good cycle stability for CO₂ reduction, and the yield of gaseous product did

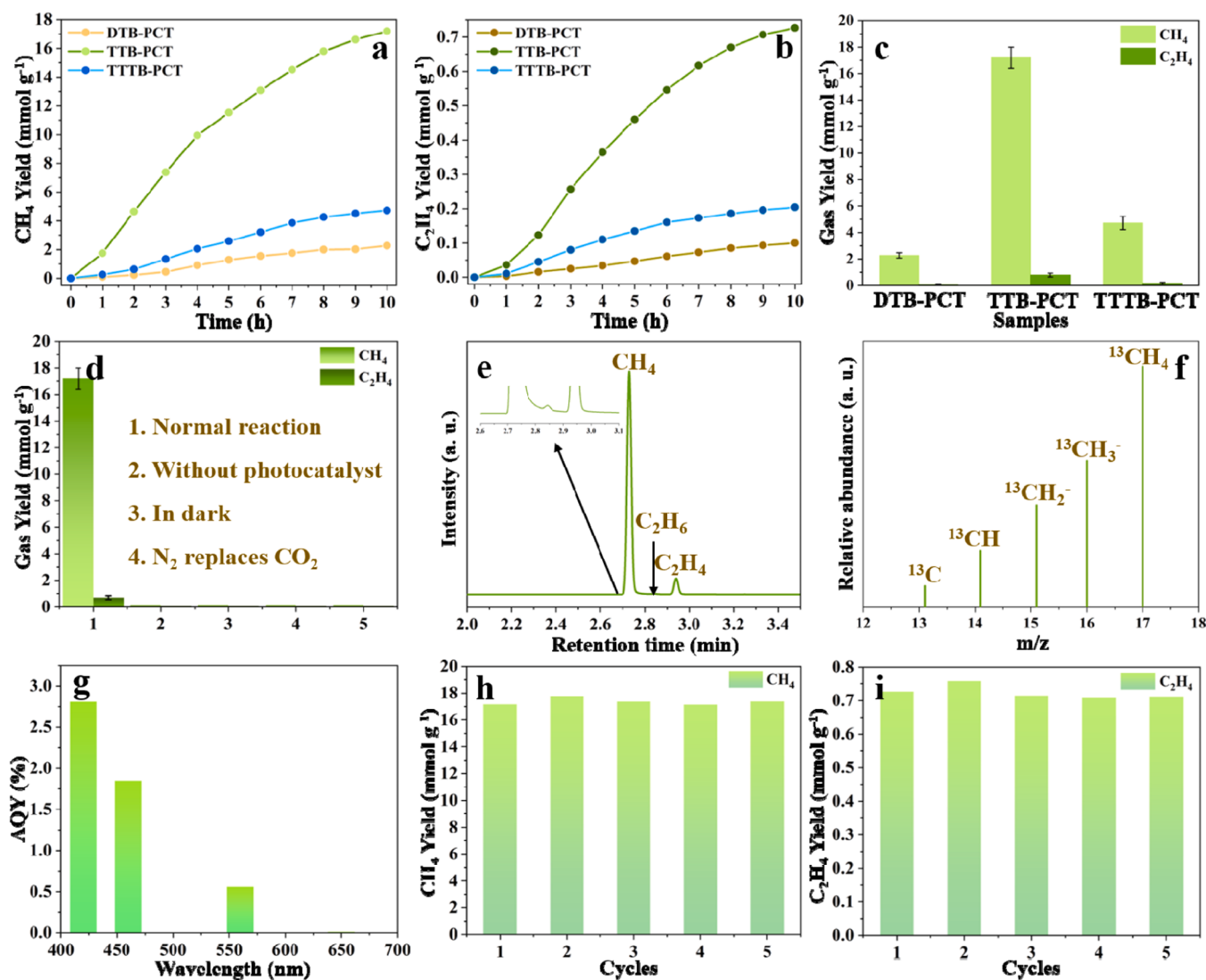


Fig. 3. (a-c) Photocatalytic conversion of CO₂ to CH₄ and C₂H₄ for DTB-PCT, TTB-PCT and TTTB-PCT. (d) Control tests to determine CH₄ and C₂H₄ production. (e) GC data of CH₄ and C₂H₄. (f) GC-MS analysis of CH₄ by using ¹³CO₂. (g) Quantum efficiency data of TTB-PCT. (h) Cycling stability test of reduce CO₂ to CH₄ based on TTB-PCT. (i) Cycling stability test of reduce CO₂ to C₂H₄ based on TTB-PCT.

not decrease significantly after five cycle tests (10 h per cycle) (Fig. 3h and i). The TTB-PCT samples were evaluated after cycling using FT-IR (Fig. S6) and XRD (Fig. S7) tests. The results showed no significant changes in the functional groups of TTB-PCT samples compared to those before cycling [33]. These findings indicate the structural stability of the TTB-PCT samples.

In order to investigate the important role of *CH₂ intermediates for the multi-electron products, the concentration of protons in the solution and thus the species of the products were changed by varying the concentration of protons in the solution. It is well known that triethanolamine (TEOA) is rich in protons [34]. Moreover, the pH in TEOA solution is a basic environment, and it is very favorable for C-C coupling [35]. We also investigated the photocatalytic reduction of CO₂ by TTB-PCT samples in pure water. Its reduction products were all CO, with a yield of 7.7 mmol g⁻¹ in 10 h (Fig. S8) and a selectivity close to 100% (Fig. S9). Control experiments showed that the addition of pure water as a sacrificial agent resulted in CO as the only product of CO₂ reduction. However, the addition of TEOA as a sacrificial agent immediately converted the product to CH₄. Acetonitrile was added to the mixed solution to further increase the adsorption of CO₂, thus greatly enhancing the CH₄ yield (Fig. S10). Based on these results, TEOA provides not only an abundance of protons but also a basic environment, which is important

for the formation and stabilization of *CH₂ intermediates leading to the final formation of CH₄ and C₂H₄ products. Similarly, we conducted control experiments that confirmed the absence of CO production without a catalyst, light and CO₂ (Fig. S11). The photocatalytic test using ¹³C-labeled CO₂ showed CO gas with skeleton fragments of 13, 16 and 29 (Fig. S12), indicating that the CO gas originated from CO₂. The TTB-PCT samples also showed consistent CO₂ reduction yields after five cycles of testing (Fig. S13), indicating their high stability.

3.3. Clarification of the proposed mechanism

The visible light absorption of DTB-PCT, TTB-PCT and TTTB-PCT samples was measured using ultraviolet-visible diffuse reflection spectroscopy (DRS) (Fig. S14). The results indicate that all three polymers had good visible light absorption. Importantly, compared to DTB-PCT, TTTB-PCT and TTB-PCT had the strongest absorption in the entire visible region. The band gaps of DTB-PCT, TTB-PCT and TTTB-PCT samples were calculated based on DRS data and found to be 1.20 eV, 1.25 eV and 1.15 eV, respectively (Fig. S15) [36]. The conduction band (CB) values of DTB-PCT, TTB-PCT and TTTB-PCT samples were -0.62 V, -0.80 V and -0.55 V (Fig. S16), respectively, for the Mott-Schottky test at different frequencies (500 KHz and 1000 KHz)

[37]. All three CPs had positive flat band potential slope values. It demonstrates that all three sample are n-type semiconductors [38]. The valence band (VB) positions were determined using XPS VB spectrum [39], and the results showed that the VB positions of DTB-PCT, TTB-PCT and TTTB-PCT were 0.58 V, 0.45 V and 0.60 V (Fig. S17), respectively. Based on the band gap diagram (Fig. S18), it was observed that the CB positions of three samples were more negative than the potential required for reducing CO₂ to CH₄ or C₂H₄, indicating the thermodynamic feasibility of catalyzing CO₂ reduction to multi-electronic products.

In order to verify the difference of photocatalytic CO₂ reduction performance among three CPs, the orbital distribution of the minimum repeat units of three samples was firstly calculated by DFT calculation. The results show that their HOMO orbitals are concentrated on the cyclotriphosphonitrile ring, while the LUMO orbitals are concentrated on the benzene ring as the central region (Fig. S19). This indicates that the cyclotriphosphonitrile and benzene ring successfully constructed the D-π-A structure with separated HOMO and LUMO orbitals through the alkyne bridge, which is beneficial to facilitate the separation of photo-generated carriers [40]. Then the molecular dipole moments of three elements were calculated (Fig. 4), and it was found that TTB-PCT had the largest molecular dipole moment (1.66 D), which was greater than

that of TTTB-PCT monomer (1.49 D) and more than twice that of DTB-PCT monomer (0.68 D). The larger the molecular dipole moment produce larger internal electric field, which could effectively promote the separation of photogenerated carriers, indicated that TTB-PCT sample had the strongest REDOX capacity, followed by TTTB-PCT and DTB-PCT samples [41]. The results are highly matched to our CO₂ reduction experimental data, indicating that the photovoltaic effect of CPs is very dependent on the modulation of alkyne bridges in their structures.

Theoretical results were validated through photocurrent, impedance, and transient fluorescence tests. TTB-PCT sample demonstrated the highest current response value (Fig. 4d), indicating efficient charge transport and participation in REDOX reactions [42]. Impedance testing revealed a smaller radius of Quist circle and lower impedance value for TTB-PCT sample (Fig. 4e), further confirming its superior charge transport efficiency. Transient fluorescence testing showed that TTB-PCT sample had the longest average fluorescence lifetime (Fig. 4f), suggesting better participation in REDOX reactions [43]. Cyclic voltammetry was employed to examine the redox behavior of TTB-PCT and its monomers (Fig. S20). The TTB monomer exhibited a significant oxidation peak at 2.77/2.81 V, accompanied by smaller reduction peaks at -1.14/-1.64 V, indicating its feature of single-electron oxidation

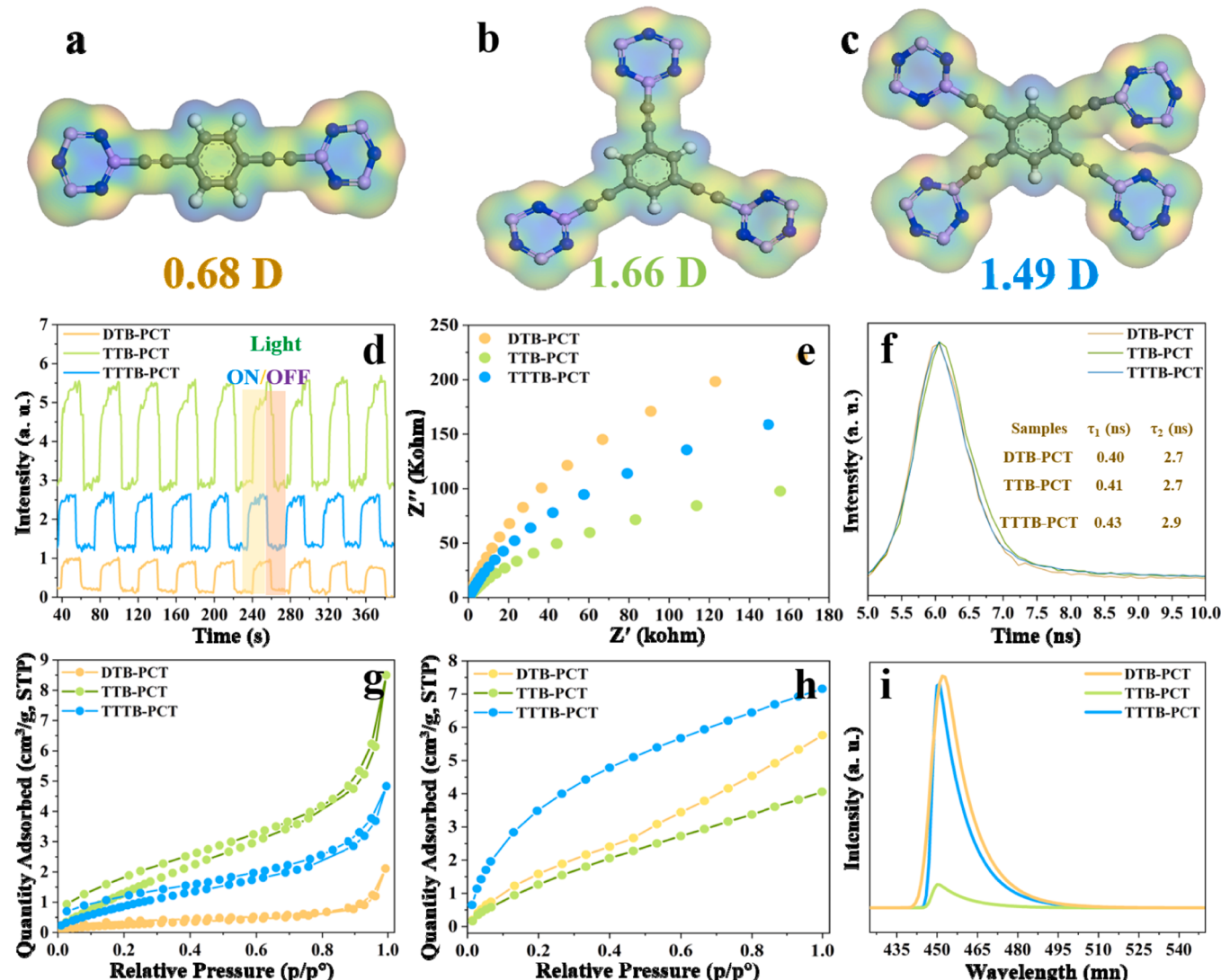


Fig. 4. The molecular dipole of (a) DTB-PCT, (b) TTB-PCT and (c) TTTB-PCT samples. (d) Photocurrents, (e) Electrochemical impedance (ESI) spectra, (f) TRPL spectra, (g) N₂ adsorption-desorption isotherm, (h) CO₂ adsorption-desorption isotherm and (i) PL spectra of DTB-PCT, TTB-PCT and TTTB-PCT.

and reduction. Similarly, PCT monomer showed a large oxidation peak at 1.18/1.35 V and two continuous reduction peaks at $-0.29/-1.12$ V and -1.37 V. TTB-PCT samples inherited the single-electron oxidation and reduction features of its monomers, with higher peaks at 2.73/2.87 V and lower peaks at $-0.91/-1.23$ V. Importantly, TTB-PCT sample demonstrated an increased oxidation capacity and a heightened reduction capacity compared to its monomers, indicating its capacity for electron loss and acquisition, respectively [44].

Then we carried out experimental verification and theoretical calculation analysis on the electron aggregation state of CPs samples. The TTB-PCT sample exhibited the largest specific surface area, followed by the TTTB-PCT sample and the DTB-PCT sample (Fig. 4g). During CO_2 adsorption experiment, the CO_2 gas adsorption capacity of TTB-PCT sample was lower than that of DTB-PCT and TTTB-PCT (Fig. 4h), which indicated that CO_2 adsorption capacity was not a documented factor to enhance the photocatalytic activity of TTB-PCT sample. In addition to the adsorption of CO_2 , the CO_2 reduction process involves

electron transfer between the catalyst and the adsorbed CO_2 molecules. Only effective electron transfer can realize CO_2 reduction. Otherwise, even if the catalyst adsorbs more CO_2 , effective CO_2 reduction cannot be realized [45]. Moreover, since the HOMO orbitals (electron-rich regions) of CPs samples are concentrated in the cyclotriphosphonitrile ring, the C atoms in the CO_2 molecules are electrostatically attracted to the cyclotriphosphonitrile ring, thus adsorbing CO_2 and key intermediates ($^*\text{CH}_2$). The fluorescence excitation test revealed notable differences between the TTB-PCT sample, DTB-PCT and TTTB-PCT samples when excited at a wavelength of 420 nm (Fig. 4i). Specifically, the fluorescence effect of TTB-PCT sample was inferior to that of other two samples. This result indicates the low photoelectron recombination probability of TTB-PCT samples as well as the fact that it exhibits excitation delay at short wavelengths due to their strong light absorption.

Density of states and charge calculations for the polymerization units of all three samples indicated that the wider peak of the density of states

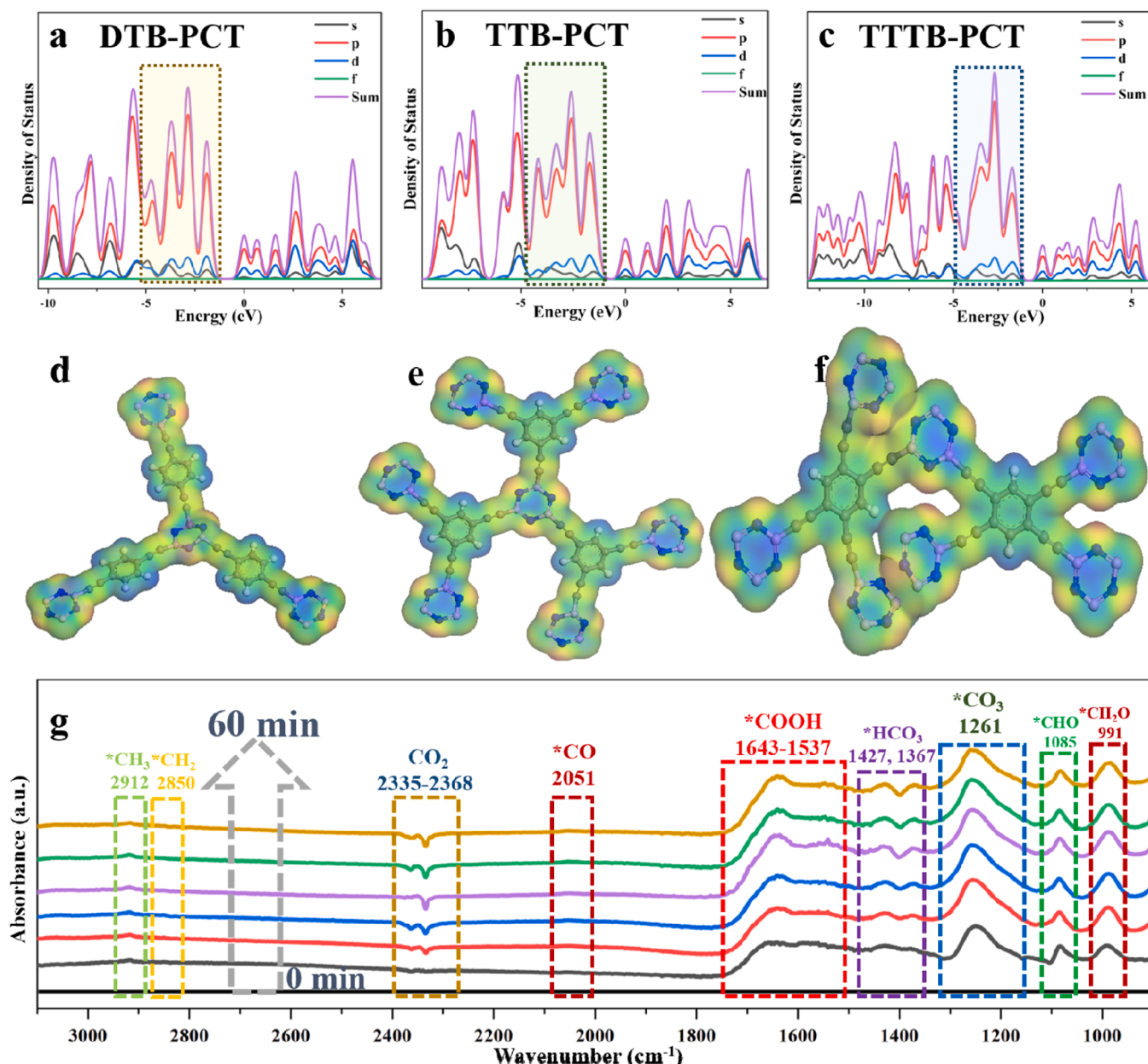


Fig. 5. TDOS results of (a) DTB-PCT, (b) TTB-PCT and (c) TTTB-PCT samples. The ESP of (d) DTB-PCT, (e) TTB-PCT and (f) TTTB-PCT samples. (g) In-situ FT-IR spectra of TTB-PCT under CO_2 atmosphere.

of DTB-PCT (Fig. 5a), TTB-PCT (Fig. 5b) and TTTB-PCT (Fig. 5c) in the low energy band region of $-6\text{--}0\text{ eV}$ indicates strong electron decentralization [46]. The DTB-PCT sample exhibits split peaks in the low-energy band region with poor electron dispersion and strong electron binding, which makes it unfavorable for photoexcitation. The density peaks of states of TTTB-PCT sample in the low-energy region are similar to those of TTB-PCT sample, as evidenced by the width of the density of states peak in the band of $-2\text{--}0\text{ eV}$. Furthermore, TTB-PCT sample shows slightly better electron delocalization (Fig. 5e) than TTTB-PCT sample (Fig. 5f) [47], which could be attributed to the thick electron cloud of TTB monomer that binds electrons to the overlapping ring edges. The DTB monomer has only two alkynes, and when it is connected to the cyclotriphosphonitrile ring, the gap between the rings is too large resulting in a low overlap between electron clouds (Fig. 5d). As a result, the electrons are bound to their respective ring edges. Only the TTB monomer has three alkynes that are connected to the cyclotriphosphonitrile with just the right distance and recombination of the electron cloud in the ring to ensure large electron planes and delocalization, which makes it more susceptible to photoexcitation to produce carriers for CO_2 reduction.

In-situ infrared spectroscopy (In-situ FTIR) is used to detect intermediates adsorbed on catalyst surfaces (TTB-PCT) in photocatalytic CO_2 reduction reactions (Fig. 5g) [48]. Absorption peaks were observed for various functional groups in the following wavenumber ranges: $^*\text{HCO}_3$ (1367 cm^{-1} and 1427 cm^{-1}), $^*\text{CO}_3$ (1261 cm^{-1}), $^*\text{CO}_2$ ($2335\text{--}2368\text{ cm}^{-1}$), $^*\text{COOH}$ ($1643\text{--}1537\text{ cm}^{-1}$), $^*\text{CO}$ (2051 cm^{-1}), $^*\text{CHO}$ (1085 cm^{-1}), and CH_2O (991 cm^{-1}) [49]. In addition to this, we observed one very important intermediate. The absorption peak of $^*\text{CH}_2$ is at 2850 cm^{-1} , which is critical for the formation of both CH_4 and C_2H_4 . Based on these key intermediates, a reduction process from CO_2 to CH_4 and C_2H_4 was proposed (Fig. S21), the energy change was calculated by DFT (Fig. 6) [50]. TTB-PCT first adsorbed with CO_2 ($\Delta G=0.078\text{ eV}$) to generate $^*\text{CO}_2$ intermediate, and then obtained electrons and hydrogen ions ($\Delta G=0.83\text{ eV}$) to generate $^*\text{COOH}$ intermediate. $^*\text{COOH}$ gains electrons and removes a water molecule to produce a $^*\text{CO}$ intermediate. At this point, the $^*\text{CO}$ intermediate gains electrons and hydrogen ions ($\Delta G=0.44\text{ eV}$) can become the $^*\text{CHO}$ intermediate, while the $^*\text{CO}$ intermediate desorbs to CO or the $^*\text{CO}\text{-}^*\text{CO}$ coupling continues to protonate to form the C_2H_4 product [51]. This shows that the electron-rich properties of TTB-PCT can adsorb and stabilize the intermediate products in the CO_2 reduction process, so as to realize the continuous reduction process of multi-electrons. However, it is thermodynamically preferred to become a $^*\text{CHO}$ intermediate. $^*\text{CHO}$ gets electrons and hydrogen ions to form $^*\text{CHOH}$ intermediate, and $^*\text{CHOH}$ intermediate gets electrons and hydrogen ions to produce $^*\text{CH}_2\text{OH}$ intermediate, which gains electrons and removes a molecule of water to

form $^*\text{CH}_2$ intermediate. The $^*\text{CH}_2$ intermediate can generate two products via two pathways. One pathway is $^*\text{CH}_2$ intermediate gains electrons and hydrogen ions to form $^*\text{CH}_3$ intermediate, $^*\text{CH}_3$ intermediate gains electrons and hydrogen ions to form CH_4 . Another pathway is that $^*\text{CH}_2$ will self-coupling to generate C_2H_4 simultaneously, due to a large number of $^*\text{CH}_2$ intermediates aggregate caused by the adsorption of electron rich TTB-PCT on $^*\text{CH}_2$. A large number of $^*\text{CO}$ and $^*\text{CH}_2$ intermediates were successfully captured by in-situ infrared, which proved the rationality of the correlation path. The transformation products CH_4 and C_2H_4 compete in a reaction, with CH_4 being produced more significantly due to its lower energy level. By adjusting the π bridge structure of D- π -A covalent polymer, the CPs are endowed with relatively prominent electron rich properties, which is conducive to stabilizing the key intermediates in the CO_2 reduction process and realizing the continuous multi-electron reduction process.

4. Conclusion

In summary, D- π -A CPs catalysts were synthesized by nucleophilic substitution under solvothermal synthesis method, in which cyclotriphosphonitrile was used as the donor part (D) and benzene ring as the acceptor unit (A), and the D and A units were isolated by alkyne bridges (π - π conjugates). Experimental results and theoretical calculations certificate that the number of π -bridges between the D and A units can well regulate the photoinduced carrier separation and reduction ability of CPs photocatalyst. The electron-rich heteroatom (P = N) in the cyclotriphosphonitrile can also serve as a Lewis site for the adsorption of CO_2 and the key intermediate ($^*\text{CH}_2$), thus providing a site for the C-C coupling reaction. Among them, the three π -bridges (TTB-PCT) exhibited excellent activity of CO_2 reduction to CH_4 (17.20 mmol g^{-1}), which was 7.6 and 3.6 times higher than that of two π -bridges (DTB-PCT) and four π -bridges (TTTB-PCT), respectively. The C-C coupling product C_2H_4 was also obtained by using the TTB-PCT catalyst with a production rate of up to 0.72 mmol g^{-1} and excellent cycling stability (50 h). This research shows a practical basis and theoretical validation for the construction of efficient D- π -A CPs catalysts through the modulation of alkyne bridges.

CRediT authorship contribution statement

Guoen Tang: Conceptualization, Data curation, Formal analysis, Investigation, Methodology, Writing – original draft. **Xiaoyan Huang:** Validation, Investigation, Formal analysis. **Ting Song:** Writing – review & editing, Conceptualization, Investigation, Formal analysis, Visualization, Funding acquisition. **Shiheng Yin:** Investigation, Writing – review & editing. **Bei Long:** Methodology, Writing review & editing. **Guo-**

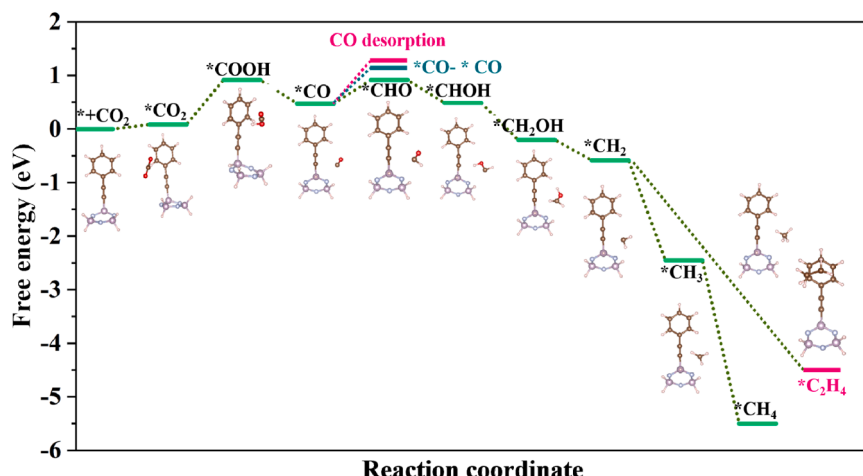


Fig. 6. Free energy diagrams for reduction of CO_2 to CH_4 and C_2H_4 over the TTB-PCT sample based on DFT calculation.

Jun Deng: Writing – review & editing, Formal analysis, Conceptualization, Investigation, Visualization.

Declaration of Competing Interest

The authors declare that they have no known competing financial interests or personal relationships that could have appeared to influence the work reported in this paper.

Data availability

Data will be made available on request.

Acknowledgements

We are extremely grateful for the financial support of General Project of Education Department of Hunan Province (21C008), Open Research Fund of School of Chemistry and Chemical Engineering, Henan Normal University (2022C02), the Hunan Provincial Natural Science Foundation of China (2021JJ40529) and the research fund of the Science and Technology Innovation Program of Hunan Province (2020RC2076).

Appendix A. Supporting information

Supplementary data associated with this article can be found in the online version at doi:10.1016/j.apcatb.2023.123392.

References

- [1] A. Zhang, P. Dong, Y. Wang, K. Gao, J. Pan, B. Yang, X. Xi, J. Zhang, Fabrication of well-dispersed pt nanoparticles onto the donor-acceptor type conjugated polymers for high-efficient photocatalytic hydrogen evolution, *Appl. Catal. B Environ.* 644 (2022) 118793–118803.
- [2] Y.Z. Cheng, W. Ji, P.Y. Hao, X.H. Qi, X. Wu, X.M. Dou, X.Y. Bian, D. Jiang, F. Li, X. F. Liu, D.H. Yang, X. Ding, B.H. Han, A. Fully, Conjugated covalent organic framework with oxidative and reductive sites for photocatalytic carbon dioxide reduction with water, *Angew. Chem. Int. Ed.* (2023), e202308523.
- [3] Q. Xu, L. Wang, X. Sheng, Y. Yang, C. Zhang, L. Duan, H. Guo, Understanding the synergistic mechanism of single atom Co-modified perovskite oxide for piezo-photocatalytic CO₂ reduction, *Appl. Catal. B Environ.* 338 (2023) 123058–123068.
- [4] I. Merino-García, S. Castro, A. Irabien, I. Hernández, V. Rodríguez, R. Camarillo, J. Rincón, J. Albo, Efficient photoelectrochemical conversion of CO₂ to ethylene and methanol using a Cu cathode and TiO₂ nanoparticles synthesized in supercritical medium as photoanode, *J. Environ. Chem. Eng.* 10 (2022) 107441–107451.
- [5] A.F.M. EL-Mahdy, H.A.E. Omr, Z.A. AL-Othman, H. Lee, Design and synthesis of metal-free ethene-based covalent organic framework photocatalysts for efficient, selective, and long-term stable CO₂ conversion into methane, *J. Colloid Interface Sci.* 633 (2023) 775–785.
- [6] H. Huang, N. Zhang, J. Xu, Y. Xu, Y. Li, J. Lü, R. Cao, Photocatalytic CO₂-to-ethylene conversion over Bi₂S₃/CdS heterostructures constructed via facile cation exchange, *Research* 2022 (2022), 9805879.
- [7] T. Wang, L. Chen, C. Chen, M. Huang, Y. Huang, S. Liu, B. Li, Engineering catalytic interfaces in Cu²⁺/CeO₂-TiO₂ photocatalysts for synergistically boosting CO₂ reduction to ethylene, *ACS Nano* 16 (2022) 2306–2318.
- [8] X. Yi, S. Zhang, H. Shen, B. Li, L. Yang, W. Dai, R. Song, J. Zou, S. Luo, Atomic sulfur dissimilation remolding ZnIn₂S₄ nanosheets surface to enhance built-internal electric field for photocatalytic CO₂ conversion to syngas, *Appl. Catal. B Environ.* 338 (2023) 123003–123013.
- [9] F. Guo, R. Li, S. Yang, X. Zhang, H. Yu, J.J. Urban, W. Sun, Designing heteroatom-codoped iron metal-organic framework for promotional photoreduction of carbon dioxide to ethylene, *Angew. Chem. Int. Ed.* 62 (2023), e202216232.
- [10] R. Das, R. Paul, A. Parui, A. Shrotri, C. Atzori, K.A. Lomachenko, A.K. Singh, J. Mondal, S.C. Peter, Engineering the charge density on an In_{2.77}S₄/porous organic polymer hybrid photocatalyst for CO₂-to-ethylene conversion reaction, *J. Am. Chem. Soc.* 145 (2023) 422–435.
- [11] R. Xu, D.H. Si, S.S. Zhao, Q.J. Wu, X.S. Wang, T.F. Liu, H. Zhao, R. Cao, Y.B. Huang, Tandem photocatalysis of CO₂ to C₂H₄ via a synergistic rhodium-(I) bipyridine/copper-porphyrinic triazine framework, *J. Am. Chem. Soc.* 145 (2023) 8261–8270.
- [12] S. Wang, M. Wang, Y. Liu, X. Meng, Y. Ye, X. Song, Z. Liang, Novel D-π-A conjugated microporous polymer as visible light-activated oxidase mimic for efficient colorimetric detection of glutathione, *Sens. Actuators B Chem.* 326 (2021), 128808.
- [13] A. Hayat, M. Sohail, U. Anwar, T.A. Taha, K.S. El-Nasser, A.M. Alenad, A.G. Al-Shehmi, N.A. Alghamdi, O.A. Al-Hartomy, M.A. Amin, A. Alhadhrami, A. Palamanit, S.K.B. Mane, W.I. Nawawi, Z. Ajmal, Enhanced photocatalytic overall water splitting from an assembly of donor-π-acceptor conjugated polymeric carbon nitride, *J. Colloid Interface Sci.* 624 (2022) 411–422.
- [14] D. Luo, T. Shi, Q. Li, Q. Xu, M. Strømme, Q. Zhang, C. Xu, Green, general and low-cost synthesis of porous organic polymers in sub-kilogram scale for catalysis and CO₂ capture, *Angew. Chem. Int. Ed.* 62 (2023), e202305225.
- [15] X. Yang, X. Lan, Y. Zhang, H. Li, G. Bai, Rational design of MoS₂@COF hybrid composites promoting C-C coupling for photocatalytic CO₂ reduction to ethane, *Appl. Catal. B Environ.* 325 (2023) 122393–122403.
- [16] Y. Xu, N. Mao, C. Zhang, X. Wang, J. Zeng, Y. Chen, F. Wang, J.X. Jiang, Rational design of donor-π-acceptor conjugated microporous polymers for photocatalytic hydrogen production, *Appl. Catal. B Environ.* 228 (2018) 1–9.
- [17] T. Bhoyer, D.J. Kim, B.M. Abraham, S. Tonda, N.R. Manwar, D. Vidyasagar, S. S. Umare, Tailoring photoactivity of polymeric carbon nitride via donor-π-acceptor network, *Appl. Catal. B Environ.* 310 (2022) 121347–121357.
- [18] Z.P. Li, T.Q. Deng, S. Ma, Z.W. Zhang, G. Wu, J.A. Wang, Q.Z. Li, H. Xia, S.W. Yang, X.M. Liu, Three-component donor-π-acceptor covalent-organic frameworks for boosting photocatalytic hydrogen evolution, *J. Am. Chem. Soc.* 145 (2023) 8364–8374.
- [19] K. Wu, X.Y. Liu, M. Xie, P.W. Cheng, J. Zheng, W. Lu, D. Li, Rational design of D-π-A-π-D porous organic polymer with polarized π for photocatalytic aerobic oxidation, *Appl. Catal. B Environ.* 334 (2023) 122847–122857.
- [20] Y.F. Wu, J.G. Li, Z.P. Shen, D.L. Wang, R.H. Dong, J.J. Zhang, Y.Z. Pan, Y. Li, D. Wang, B.Z. Tang, Double-pronged antimicrobial agents based on a donor-π-acceptor type aggregation-induced emission luminogen, *Angew. Chem. Int. Ed.* 61 (2022), e202212386.
- [21] R. Oshimizu, N.K. Ando, S.H. Yamaguchi, Olefin–borane interactions in donor-π-acceptor fluorophores that undergo frustrated-lewis-pair-type reactions, *Angew. Chem. Int. Ed.* 61 (2022), e2022093.
- [22] C. Han, S. Xiang, S. Jin, C. Zhang, J.X. Jiang, Rational design of conjugated microporous polymer photocatalysts with definite D-π-a structures for ultrahigh photocatalytic hydrogen evolution activity under natural sunlight, *ACS Catal.* 13 (2023) 204–212.
- [23] S. Choi, Y.J. Kim, S. Kim, H.S. Lee, J.Y. Shin, C.H. Kim, H.J. Son, S.O. Kang, Outer-sphere electron-transfer process of molecular donor-acceptor organic dye in the dye-sensitized photocatalytic system for CO₂ reduction, *ACS Appl. Energy Mater.* 5 (2022) 10526–10541.
- [24] S. Barman, A. Singh, F.A. Rahimi, T.K. Maji, Metal-free catalysis: a redox-active donor-acceptor conjugated microporous polymer for selective visible-light-driven CO₂ reduction to CH₄, *J. Am. Chem. Soc.* 143 (2021) 16284–16292.
- [25] Z. Tang, S. Xu, N. Yin, Y. Yang, Q. Deng, J. Shen, X. Zhang, T. Wang, H. He, X. Lin, Y. Zhou, Z. Zou, Reaction Site designation by intramolecular electric field in tröger's-base-derived conjugated microporous polymer for near-unity selectivity of CO₂ photoconversion, *Adv. Mater.* 35 (2023), 2210693.
- [26] S. Guo, H. Zhang, Y. Chen, Z. Liu, B. Yu, Y. Zhao, Z. Yang, B. Han, Z. Liu, Visible-light-driven photoreduction of CO₂ to CH₄ over N, O, P-containing covalent organic polymer submicrospheres, *ACS Catal.* 8 (2018) 4576–4581.
- [27] X. Lan, X. Liu, Y. Zhang, Q. Li, J. Wang, Q. Zhang, G. Bai, Unveiling charge dynamics in acetylene-bridged donor-π-acceptor covalent triazine framework for enhanced photoredox catalysis, *ACS Catal.* 11 (2021) 7429–7441.
- [28] A.F. Saber, A.M. Elewa, H.H. Chou, A.F.M. EL-Mahdy, Donor-acceptor carbazole-based conjugated microporous polymers as photocatalysts for visible-light-driven H₂ and O₂ evolution from water splitting, *Appl. Catal. B Environ.* 316 (2022) 121624–121634.
- [29] S. Wang, X. Hai, X. Ding, S. Jin, Y. Xiang, P. Wang, B. Jiang, F. Ichihara, M. Oshikiri, X. Meng, Y. Li, W. Matsuda, J. Ma, S. Seki, X. Wang, H. Huang, Y. Wada, H. Chen, J. Ye, Intermolecular cascaded π-conjugation channels for electron delivery powering CO₂ photoreduction, *Nat. Commun.* 11 (2020) 1149–1159.
- [30] Y. Wang, M. Liu, G. Gao, Y. Yang, R. Yang, H. Ding, Y. Chen, S. Li, Y. Lan, Implanting numerous hydrogen-bonding networks in a Cu-porphyrin-based nanosheet to boost CH₄ selectivity in neutral-media CO₂ electroreduction, *Angew. Chem. Int. Ed.* 60 (2021) 21952–21958.
- [31] J. Zhou, J. Li, L. Kan, L. Zhang, Q. Huang, Y. Yan, Y.F. Chen, J. Liu, S.L. Li, Y. Q. Lan, Linking oxidative and reductive clusters to prepare crystalline porous catalysts for photocatalytic CO₂ reduction with H₂O, *Nat. Commun.* 13 (2022) 4681–4691.
- [32] Y.F. Mu, J.S. Zhao, L.Y. Wu, K.Y. Tao, Z.L. Liu, F.Q. Bai, D.C. Zhong, M. Zhang, T. B. Lu, Lead-free halide perovskite hollow nanospheres to boost photocatalytic activity for CO₂ reduction, *Appl. Catal. B Environ.* 338 (2023) 123024–123034.
- [33] X. Yi, S. Zhang, H. Shen, B. Li, L. Yang, W. Dai, R. Song, J. Zou, S. Luo, Atomic sulfur dissimilation remolding ZnIn₂S₄ nanosheets surface to enhance built-internal electric field for photocatalytic CO₂ conversion to syngas, *Appl. Catal. B Environ.* 338 (2023) 123003–123013.
- [34] W. Dong, Z. Qin, K. Wang, Y. Xiao, X. Liu, S. Ren, L. Li, Isomeric oligo(phenylenevinylene)-based covalent organic frameworks with different orientation of imine bonds and distinct photocatalytic activities, *Angew. Chem. Int. Ed.* 62 (2023), e202216073.
- [35] S. Chakraborty, R. Das, M. Riyaz, K. Das, A.K. Singh, D. Bagchi, C.P. Vinod, S. C. Peter, CuGaS₂ with an in-situ-formed CuO layer photocatalyzes CO₂ conversion to ethylene with high selectivity, *Angew. Chem. Int. Ed.* 135 (2023), e202216613.
- [36] L.Q. Hou, Z.Y. Tang, G.J. Mao, S.H. Yin, B. Long, T. Ouyang, G.J. Deng, A. Ali, T. Song, Ultrathin organic polymer with p-π conjugated structure for simultaneous photocatalytic disulfide bond generation and CO₂ reduction, *J. Energy Chem.* 76 (2023) 639–647.

[37] Y.Z. Qian, H.R. Wang, X.N. Li, T. Song, Y. Pei, L. Liu, B. Long, X.W. Wu, X.Y. Wang, Sn-doped BiOCl nanosheet with synergistic H^+/Zn^{2+} co-insertion for “rocking chair” zinc-ion battery, *J. Energy Chem.* 81 (2023) 623–632.

[38] L.J. Chen, T.T. Liu, S.M. Liu, S. Cai, X.X. Zou, J.W. Jiang, Z.Y. Mei, G.F. Zhao, X. F. Yang, H. Guo, S vacant CuIn₅S₈ confined in a few-layer MoSe₂ with interlayer-expanded hollow heterostructures boost photocatalytic CO₂ reduction, *Rare Met.* 41 (2022) 144–154.

[39] Q.J. Xu, J.W. Jiang, X.F. Wang, L.Y. Duan, H. Guo, Understanding oxygen vacant hollow structure CeO₂@In₂O₃ heterojunction to promote CO₂ reduction, *Rare Met.* 42 (2023) 1888–1898.

[40] J.W. Jiang, X.F. Wang, H. Guo, Enhanced interfacial charge transfer/separation by LSPR-induced defective semiconductor toward high Co₂RR performance, *Small* 19 (2023), 2301280.

[41] J. Yang, J. Jing, F.Y. Zhu, A full-spectrum porphyrin–fullerene D–A supramolecular photocatalyst with giant built-in electric field for efficient hydrogen production, *Adv. Mater.* 33 (2021), 2101026.

[42] M. Kou, Y. Wang, Y. Xu, L. Ye, Y. Huang, B. Jia, H. Li, J. Ren, Y. Deng, J. Chen, Y. Zhou, K. Lei, L. Wang, W. Liu, H. Huang, T. Ma, Molecularly engineered covalent organic frameworks for hydrogen peroxide photosynthesis, *Angew. Chem. Int. Ed.* 61 (2022), e202200413.

[43] Y. Tang, Y. Li, W. Bao, W. Yan, J. Zhang, Y. Huang, H. Li, Z. Wang, M. Liu, F. Yu, Enhanced dry reforming of CO₂ and CH₄ on photothermal catalyst Ru/SrTiO₃, *Appl. Catal. B Environ.* 338 (2023) 123054–123064.

[44] C. Yang, Y. Zhang, F. Yue, R. Du, T. Ma, Y. Bian, R. Li, L. Guo, D. Wang, F. Fu, Co doping regulating electronic structure of Bi₂MoO₆ to construct dual active sites for photocatalytic nitrogen fixation, *Appl. Catal. B Environ.* 338 (2023) 123057–123067.

[45] Y.L. Dong, H.R. Liu, S.M. Wang, G.W. Guan, Q.Y. Yang, Immobilizing isatin-schiff base complexes in NH₂-UiO-66 for highly photocatalytic CO₂ reduction, *ACS Catal.* 13 (2023) 2547–2554.

[46] X. Li, Y. Huang, W. Ho, S. Han, P. Wang, S. Lee, Z. Zhang, Modulation of sulfur vacancies at ZnIn₂S₄-δ/g-C₃N₄ heterojunction interface for successive C-H secession in photocatalytic gaseous formaldehyde complete oxidation, *Appl. Catal. B Environ.* 338 (2023) 123048–123058.

[47] L. Sun, X. Liu, Y. Feng, X. Ding, J. Wang, N. Jiang, S. Wang, High loads of rare earth single-atom lanthanum anchored carbon nitride with special double-layer coordination structure for efficient photocatalysis, *Appl. Catal. B Environ.* 338 (2023) 122979–122989.

[48] Y. Zhou, Q. Zhou, H. Liu, W. Xu, Z. Wang, S. Qiao, H. Ding, D. Chen, J. Zhu, Z. Qi, X. Wu, Q. He, L. Song, Asymmetric dinitrogen-coordinated nickel single-atomic sites for efficient CO₂ electroreduction, *Nat. Commun.* 14 (2023) 3776–3786.

[49] Y. Yang, H.Y. Zhang, Y. Wang, L.H. Shao, L. Fang, H. Dong, M. Lu, L.Z. Dong, Y. Q. Lan, F.M. Zhang, Integrating enrichment, reduction, and oxidation sites in one system for artificial photosynthetic diluted CO₂ reduction, *Adv. Mater.* 33 (2023), 230417.

[50] C. Ning, J. Yang, S. Bai, G. Chen, G. Liu, T. Shen, L. Zheng, S. Xu, X. Kong, B. Liu, Y. Zhao, Y. Song, An efficient intercalation supramolecular structure for photocatalytic CO₂ reduction to ethylene under visible light, *Adv. Funct. Mater.* (2023), 2300365.

[51] X. Yang, X. Lan, Y. Zhang, H. Li, G. Bai, Rational design of MoS₂@COF hybrid composites promoting C-C coupling for photocatalytic CO₂ reduction to ethane, *Appl. Catal. B Environ.* 325 (2023) 122393–122403.